sustainability

MDPI

Article

Performance of Alkali-Activated Materials Using Precursors with High Impurity Contents

Reza Mirmoghtadaei [1], Lin Shen [1,*], Ian Jehn [2] and Baomin Wang [3]

[1] Department of Civil and Environmental Engineering, University of Hawaii at Manoa, Honolulu, HI 96822, USA
[2] Department of Civil and Environmental Engineering, Colorado School of Mines, Golden, CO 80401, USA
[3] School of Civil Engineering, Dalian University of Technology, Dalian 116024, China
* Correspondence: linshen@hawaii.edu

Abstract: The presence of impurities, such as anhydrite (calcium sulfate) and unburnt carbon, in fly ash and other industrial wastes greatly limits the utilization of these materials in the construction industry. In addition, alkali-activated materials using precursors with high impurity contents should be closely monitored to ensure long-term durability. This study investigates the performance of alkali-activated materials using precursors with high impurity contents. Successful alkali-activated mixes have been developed and comprehensive tests have been conducted on the mechanical properties, volume stability, and durability. The research determined that a new mixing procedure could significantly enhance various properties of high-impurity alkali-activated materials (HI-AAMs). The study investigated both short- and long-term mechanical properties, as well as the durability of the specimens. The hardened samples exhibited reasonable 28-day compressive strength (38 MPa (5500 psi)), and rapid strength gain (28 MPa (4000 psi)), after 3 days. HI-AAMs also demonstrated acceptable long-term properties: drying shrinkage similar to that of normal concrete after four months; resistance to 5% sodium sulfate after 180 days of exposure; passing the ASTM 1260 ASR test, and smaller creep values compared to conventional concrete samples with similar compressive strengths. With similar or even superior performances to ordinary Portland cement (OPC), HI-AAMs could be a sustainable building material suitable for a host of structural and non-structural applications. Therefore, employment of the novel mixing procedure is recommended in fabricating AAMs with high impurity contents to optimize performance, cost, and environmental benefits.

Keywords: alkali-activated materials; geopolymer; impurity; compressive strength; sulfate attack; ASR; creep

check for updates

Citation: Mirmoghtadaei, R.; Shen, L.; Jehn, I.; Wang, B. Performance of Alkali-Activated Materials Using Precursors with High Impurity Contents. *Sustainability* **2023**, *15*, 3319. https://doi.org/10.3390/su15043319

Academic Editors: Yu Song, Xu Chen and Ratana Hay

Received: 11 December 2022
Revised: 31 January 2023
Accepted: 6 February 2023
Published: 10 February 2023

Copyright: © 2023 by the authors. Licensee MDPI, Basel, Switzerland. This article is an open access article distributed under the terms and conditions of the Creative Commons Attribution (CC BY) license (https://creativecommons.org/licenses/by/4.0/).

1. Introduction

Over the past decades, great efforts have been made to develop alternative construction materials, which could significantly reduce the CO_2 emission from cement production [1–3]. Alkali-activated binders with appreciable mechanical strength and durability have shown to be a potential alternative to traditional Portland cement-based mixes. This type of cement-like binder is commonly named a geopolymer. Geopolymers consist of repeating chemical groups, such as -Si-O-Si-O- or -Si-O-Al-O-, created by the process of geopolymerization. The mechanism of geopolymerization consists of (1) the dissolution of aluminum and silicon species from source materials into solution, (2) the polymerization of these species in solution, and (3) the precipitation of a hardened gel from the solution [4–6].

To reduce the costs and environmental impacts, industrial waste materials such as coal fly ash and slag are usually used to develop geopolymers [7]. These raw materials typically contain high contents of calcium oxide and certain amounts of sulfates, chlorides, and heavy metals, which significantly differentiate geopolymer products from those obtained

with pure aluminosilicate materials. C-S-H and C-A-S-H phases, like those formed by the hydration of Portland cement, usually form in geopolymers due to the high Ca content in slag, while a pure aluminosilicate polymer network will be produced when aluminosilicate fly ash is used [8].

Researchers have encountered challenges in implementing alkali-activated products in their studies and tried to resolve the issues differently. Shi et al. [9] used cenospheres (CP) as a partial replacement for fly ash (FA) to prepare ultra-lightweight foamed geopolymer concrete (UFGC). Their results showed that adding CP to the slag-FA binder reduced the setting time and heat of alkali activation. The flowability of alkali-activated materials is the main concern when using waste materials as the precursor of AAMs. The results of another study [10] showed that air-cooled blast furnace slag significantly enhanced the fresh and hardened properties of AAMs.

One of the primary reasons why this type of binder with great short- and long-term properties cannot be utilized on a large scale is due to the low-strength geopolymer concrete cured at ambient temperatures [11]. Scholars have tried to use different fibers, admixtures, and adhesives to modify the properties of alkali-activated fly ash [12]. Some percentages of high-calcium fly ash were replaced by OPC to improve the early compressive strength [13]. Adding cotton fabrics and replacing some parts of the fly ash with OPC could enhance the mechanical and the thermal properties of geopolymer composites [14]. The long-term compressive strength of high-calcium alkali-activated binders significantly depends on the percentage of calcium in the source material. The presence of calcium hydroxide above 10% decreases the long-term compressive strength [15]. Temuujin et al. introduced CaO and $Ca(OH)_2$ to improve the mechanical properties of fly ash-based geopolymers, achieving a compressive strength of less than 30 MPa at ambient temperatures [16].

The presence of impurities, such as anhydrite (calcium sulfate) and unburnt carbon, in fly ash and other industrial wastes greatly limit the utilization of these materials in the construction industry. In addition, alkali-activated materials using precursors with high impurity contents should be closely monitored to ensure long-term durability. There is limited information in the literature about AAMs fabricated using precursors with high impurities. This research employed a simple and novel mixing procedure to effectively dissolve fly ash with high impurity contents. The short- and long-term mechanical properties of AAM samples were then compared with OPC concrete. Successful AAM specimens were made using 100% Hawaiian coal fly ash (HCF) with high impurity contents, which is not allowed to be used in OPC. The fly ash received from the supplier, without any further treatment, was mixed with sodium hydroxide and sodium silicate solutions and cured at room temperature. The new mixing procedure to fabricate the specimens could significantly enhance fresh properties, short- and long-term mechanical properties, as well as durability. This novel method could potentially provide a viable option to replace Portland cement with industrial wastes with high impurity contents, which otherwise would have to be landfilled.

2. Materials and Methods

2.1. Materials

A fly ash (AES fly ash) with high impurity contents was obtained from a local Hawaiian power plant (AES power plant, Honolulu, HI, USA) and was used to prepare samples without further treatment. The study also used ASTM C150-07 Type I/II (low-alkali) Portland cement (Hawaiian cement), class F fly ash, and Grade 120 slag (Diversified Minerals Inc., Oxnard, CA, USA). Portland cement, class F fly ash, and slag were used to fabricate samples to be compared with AES-based AAMs. The chemical compositions of these raw materials discerned by X-ray fluorescence (XRF) are shown in Table 1.

Table 1. Chemical composition of raw materials.

XRF Total Chemical Oxides	X-ray Fluorescence Oxides (%w) after Normalization			
	AES Fly Ash	**Commercial FA (Type F)**	**Slag**	**Cement**
Al_2O_3	18.20	34.73	14.87	3.01
SiO_2	38.13	53.01	31.89	17.00
CaO	21.25	2.38	41.28	65.40
Na_2O	0.28	0.29	0.13	0.27
K_2O	0.99	1.12	0.34	0.43
Fe_2O_3	6.32	4.15	0.67	3.31
TiO_2	0.72	1.17	0.44	0.72
SO_3	8.79	0.47	2.53	3.52
MgO	0.92	0.85	6.24	3.10
P_2O_5	0.49	0.28	0.05	0.09
Cl	0.00	0.00	0.00	0.00
ZnO	0.00	0.00	0.00	0.01
Sb_2O_3	0.00	0.00	0.00	0.00
MnO_2	0.04	0.04	0.29	0.05
PbO	0.00	0.00	0.00	0.00
Br	0.00	0.00	0.00	0.00
SrO	0.09	0.09	0.05	0.05
BaO	0.10	0.09	0.00	0.04
LOI *	3.69	1.35	1.22	3.00
Total	100.00	100.00	100.00	100.00

* Loss On Ignition.

AES fly ash can be defined as "high-calcium" or class C fly ash since the CaO content was higher than 10%. Oven-dried (OD) basalt sand was used to prepare mortar samples. Sodium hydroxide (NaOH) pellets with 99% purity (Fisher Scientific, Waltham, MA, USA) were used as an activator and sodium silicate solution (PQ Corporation (Malvern, PA, USA)) (Table 2).

Table 2. D-Grade sodium silicate specifications provided by the manufacturer.

Sodium Silicate Name	D-Grade™
SiO_2/Na_2O (mass ratio)	2.0
% SiO_2	29.4
% Na_2O	14.7

Table 3 shows the mix design adopted from a previous study [11] and used to prepare samples for durability tests.

Table 3. Mix design of AES fly ash mortar.

Mix Design Parameter	Ratios
S/B	0.4
SSS/S	0.2

Table 3. *Cont.*

Mix Design Parameter	Ratios
N/S	0.16
Sand/FA	1

S = total solution including sodium hydroxide, sodium silicate solutions, and water; B = binder N = NaOH pellets; FA = AES fly ash; SSS = sodium silicate solution.

The sample preparation procedure was as follows: Step 1, sodium hydroxide pellets were dissolved in water at least three hours prior to the experiment; Step 2, the sodium hydroxide solution was mixed with fly ash until a consistent paste was achieved (see Section 2.2 for a novel method of determining the appropriate timing); Step 3, sand (or aggregate in case of fabricating concrete) was added to the mix; Step 4, the sodium silicate solution was poured into the mortar (or concrete) (Figure 1).

Figure 1. The mixer (Hobart N50 mixer with 50 qt capacity with three speeds) used to fabricate the mortar samples.

Figure 2 illustrates the research steps in this study, and each step will be discussed in depth in the following sections.

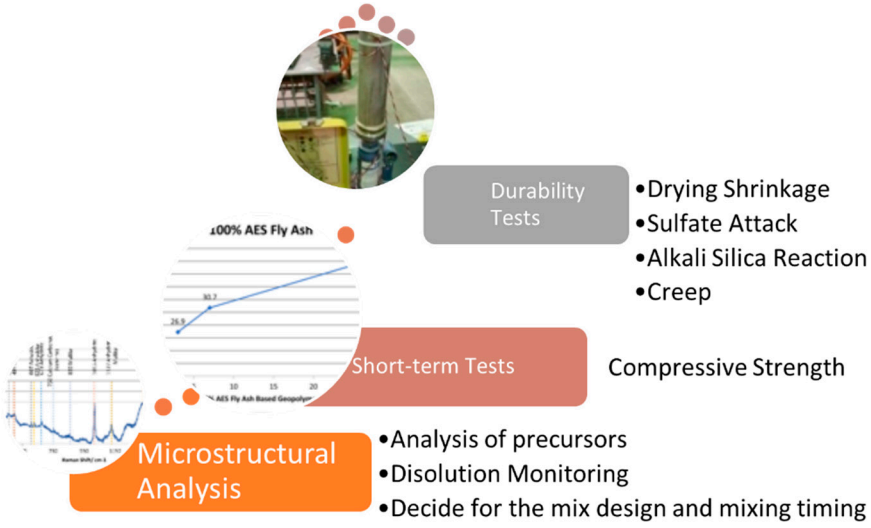

Figure 2. Summary of the research steps.

2.2. A Novel Method of Determining the Appropriate Timing

Raman spectroscopy can be used to determine any crystalline or amorphous phase at any moment after mixing [11]. Figure 3 illustrates the phases of AES fly ash. The dissolution process started after the sodium hydroxide solution was introduced to the precursors, and intensity changes in peaks and regions of interest were continuously monitored for up to 24 h. Measurements were taken every 1 min for the first 90 min, and then every 30 min until the completion of the experiment.

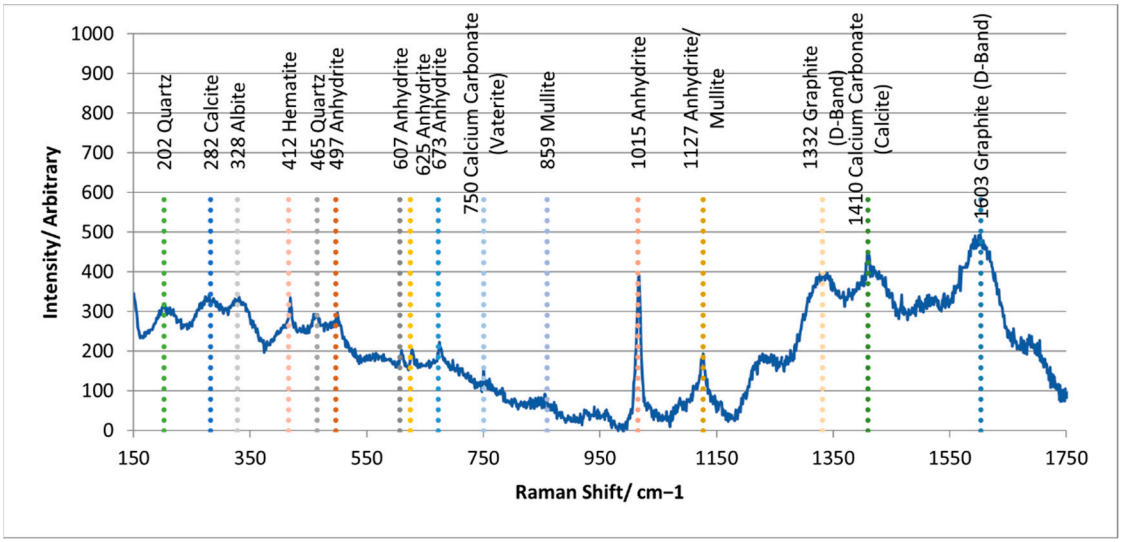

Figure 3. Raman spectroscopy of the AES fly Ash.

It was found that both the crystalline and glassy constituent parts of the AES fly ash were dissolved within the first 20 min. Due to the reformation of molecules, intensities increased during nearly the same period. The optimum mixing time of AES fly ash with sodium hydroxide was determined to be 12 min when the anhydrite and graphite (impurities) peaks flatten. The details of this novel method are discussed elsewhere [11].

2.3. Comprehensive Tests of the Mechanical Properties, Volume Stability, and Durability

The fresh and short-term sample properties were satisfactory and were discussed in a previous study [4]. Since it is crucial to verify the long-term performances of mixes with high impurities, samples were subjected to further tests of mechanical properties, volume stability, and durability, which will be the focus of this research. Standard tests included compressive strength (ASTM C39), sulfate exposure testing (ASTM C1012), potential alkali–silica reaction (ASTM C1260), shrinkage (ASTM C157), and creep (ASTM C512).

2.3.1. Compressive Strength

For compressive strength tests, fresh mortar (or concrete) was cast into 50.8 × 50.8 × 50.8 mm brass molds (polyvinyl chloride (PVC) molds to form 101.6 mm (diameter) × 203.2 mm (high) cylinders for concrete samples) (Figure 4) and carefully compacted to minimize the amount of entrapped air. Demolding of the specimens was completed after 24 h at room temperature and then moisture-cured (20 ± 2 °C, relative humidity: 95%) (Figure 5) for additional days. ASTM C39 was followed to conduct the compressive strength tests with a loading rate of 0.5 mm/min. An average measurement of three strength values was used for each sample set's compressive strength.

Figure 4. (**a**) brass mold to fabricate the mortar samples. (**b**) PVC mold to fabricate the concrete samples.

Figure 5. Moisture cure of the samples.

A Compression Tester (Accu-tek (CT-7500Series, capacity: 500,000 lbf./2225 kN, accuracy: +/−1%)) (Figure 6) was used to measure the compressive strength of the alkali-activated mortar and concrete samples. The compressive strength of most of the specimens was measured at 3, 14, and 28 days after casting. Three specimens were tested after 3, 7, and 28 days of curing. (see Figure 7 for the failure type selection).

Figure 6. Compression machine.

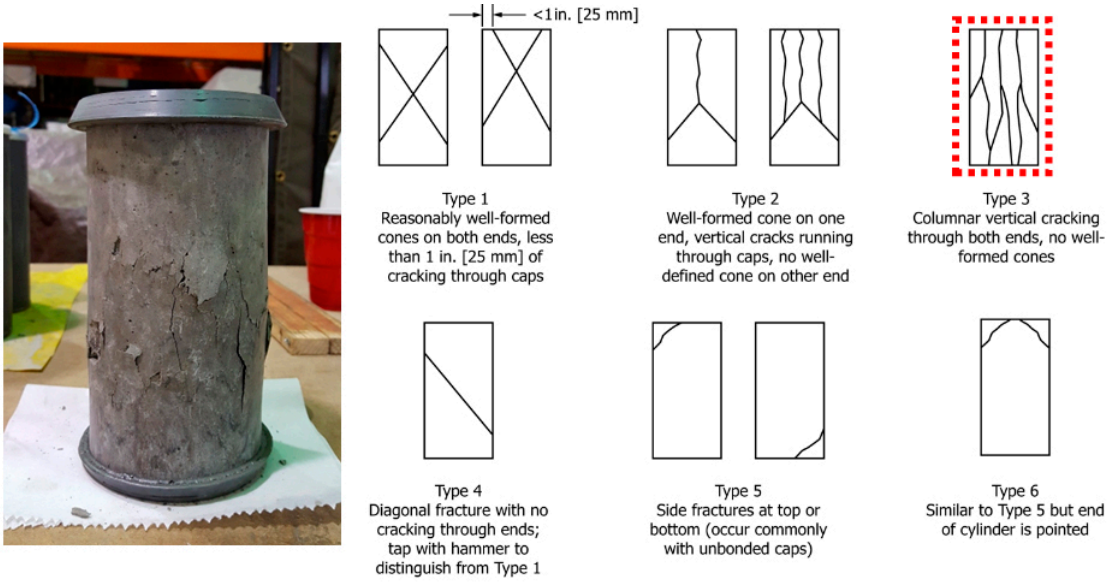

Figure 7. Failure type selection.

2.3.2. Sulfate Exposure Testing

The testing procedure was based on the mortar bar method per ASTM C1012 as described below:

Shrinkage test—ASTM C1012—length change in hardened hydraulic-cement mortar exposed to a sulfate solution.

Testing procedure:

1. Four bar specimens were prepared for each sample set. Based on the ASTM code, data from three bars must be available for the test to be valid (Figure 8);
2. With the same mix, mortar cubes were cast and tested for compression testing. Three cubes were fabricated for each sample set for anticipated compression testing throughout the test (Figure 9);
3. Test specimens were covered and cured in molds at 35 ± 0.1 °C for 23.5 ± 0.5 h;
4. Specimens were removed from the molds and placed in lime-saturated water at 23.5 ± 0.1 °C. The first two cubes were tested to determine if the compressive strength exceeded 3000 psi. If not, bars and cubes had to be submerged until the compressive strength reached 3000 ± 150 psi.

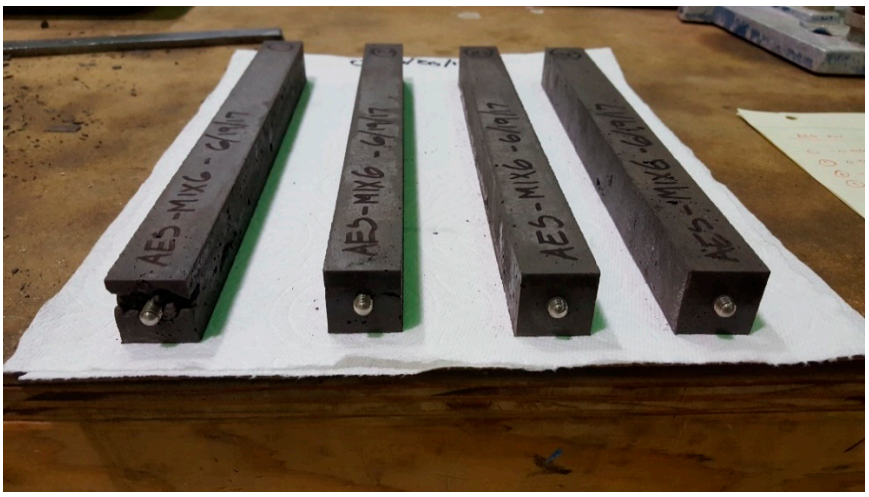

Figure 8. Bar specimens based on the ASTM C490 requirements.

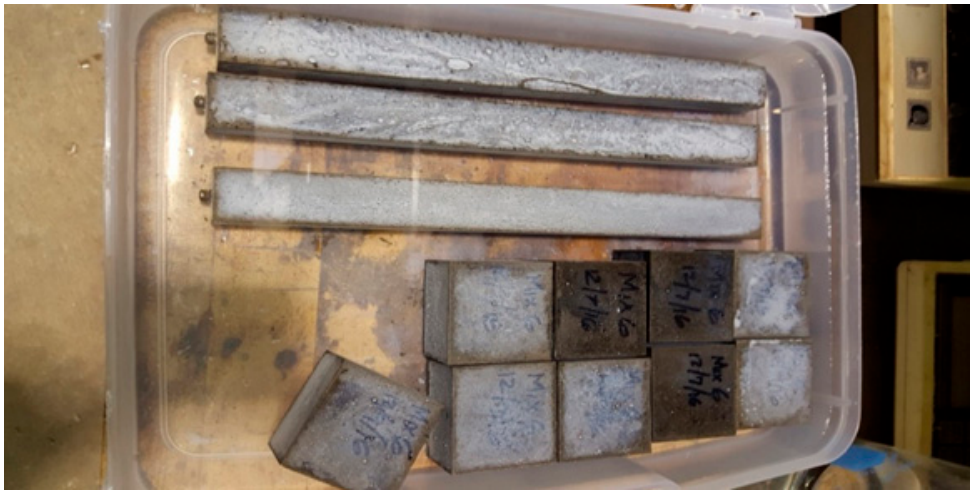

Figure 9. Test setup for sulfate-exposure testing.

It should be noted that 2 g/L of calcium hydroxide ($Ca(OH)_2$—hydrated lime) was used to prepare the saturated lime-curing water. The compressive strength was taken as the average of three specimens.

- ❖ After strength was achieved, a caliper was used to measure the initial length of the fully submerged bars and cubes in sulfate solutions.
- ❖ Based on the ASTM standard: The solution should contain 50 g of sulfate dissolved in 900 mL of deionized water, and the solution should be diluted until the solution reaches 1.0 L;
- ❖ The volume of sulfate solution was proportionate to the specimen by 4.0 ± 0.5 volumes;
- ❖ Each solution container was sealed to prevent evaporation;
- ❖ Additional comparator readings were taken when the specimen had been submerged for a period of 1, 2, 3, 4, 8, 13, and 15 weeks, then 4, 6, 9, 12, 15, and 18 months. Additionally, on the same measurements date, test cube specimens were tested, and any changes in compressive strength were recorded. Each specimen was examined while measuring, and any changes (warping, cracking, surface deposits, mottling, or exudations) were documented.
- ❖ The length changes were calculated as:

$$\Delta L = \left[\frac{L_x - L_i}{G}\right] 100 = \% \text{ change in length}$$

In which: Li = initial length Lx = length at time X G = length between gage studs = 10″

2.3.3. Potential Alkali–Silica Reactions

The following procedure was based on the mortar bar method as per ASTM C1260:

1. Both the molds and comparator apparatus (Humboldt digital length comparator with the bar dimension of 7-1/2″ w. × 7-3/4″ d. × 17-3/4″ h. (190 × 197 × 451 mm) and 0.0001″ accuracy) described in ASTM C490 were used for the testing procedure (Figure 10);
2. Reactive aggregates were selected for the proposed testing;
3. Aggregates were prepared using the grading requirements shown in Table 4;

Table 4. Grading requirements.

Sieve Size		Mass, %
Passing	**Retained on**	
4.75 mm (No. 4)	2.36 mm (No. 8)	10
2.36 mm (No. 8)	1.18 mm (No. 16)	25
1.18 mm (No. 16)	600 µm (No. 30)	25
600 µm (No. 30)	300 µm (No. 50)	25
300 µm (No. 50)	150 µm (No. 100)	15

Figure 10. Test setup for potential alkali–silica reaction testing.

4. Mortar samples were proportioned to 1 part binder to 2.25 parts graded aggregate by mass;
5. Three-bar specimens were mixed and molded using two equal layers. Each layer was compacted and finished flush with the mold;
6. Test specimens were cured in the molds with 95% humidity at 75 °F for 24 ± 2 h;
7. Specimens were demolded and placed in a tap water container at 74 ± 4 °F;
8. The container was placed in an oven at 176 ± 3 °F for 24 h;
9. After 24 h, an initial reading of specimens was taken in the comparator;
10. Specimens were stored in a container with 1N of NaOH at 176 ± 3 °F and placed back in the oven. Containers needed to be sealed to prevent evaporation of the solution in the oven:
    - ❖ 1N = 1 normal solution. N = mol weight/1.0.
    - ❖ [NaOH] = 40 g/mol
    - ❖ $1N_{[NaOH]}$ = 40 g/L
11. Three readings were taken within 14 days of being submerged in the solution;

12. Additional readings were taken beyond 14 days at a rate of once per week;
13. It was ensured that the solution did not evaporate below the level of the specimen. In this way, specimens were fully submerged at all times;
14. Record length change was calculated and recorded as:

$$\Delta L = \left[\frac{L_x - L_i}{G}\right] 100 = \% \text{ change in length}$$

In which:

Li = initial length
Lx = length at time X
G = length between gage studs = 10″

15. Limits of expansion:
    - Expansions of less than 0.10% at 16 days after casting were considered as an indication of innocuous behavior in most cases;
    - Expansions of more than 0.20% at 16 days after casting were considered as an indicator of potentially deleterious expansion;
    - Expansions between 0.10 and 0.20% at 16 days after casting including both aggregates were known to be innocuous and deleterious for in-field performance.

2.3.4. Creep

The philosophy of this test was to use the AAMs using AES fly ash (class C with high impurities) and run the ASTM C512 "Standard Test Method for Creep of Concrete in Compression".

The molds used were 6″ × 12″ cylinders, conforming to the ASTM C192 and C470. Six specimens were needed from a given batch per ASTM C192 and C470. Wire strain gauges (Geokon strain gauge model 4200L with ±0.5% FS accuracy, Geokon, Lebanon, NH, USA) were vibrated to be embedded into the three specimens. Further, gauges were installed as per the manufacturer's specifications. Test specimens were cured in covered molds to prevent evaporation at 73.5 ± 3.5 °F for 20 to 48 h. Specimens were removed afterwards from the molds and cured in moist conditions (not submerged) at 50% humidity and 73.5 ± 3.5 °F for 28 days. The average of the two cylinders' compressive strength was recorded for the samples at 28 days. At this stage, the intensity of the loading applied to cylinders was determined (see Figure 11 for the test setup).

Specimens were not loaded (MTS Systems Corporation, Eden Prairie, MN, USA) load cell with 25 M.T. capacity) with more than 40% of their 28-day compressive strength. Two specimens with embedded strain gauges in the loading frame were installed, matching the description in the mentioned standard. Strain readings were obtained immediately before and after loading in the frame. The investigation recorded the strain two to six hours after loading and then daily for one week, weekly for one month, and monthly for one year. If the load in a frame varied more than 2% from the correct values, it was immediately adjusted.

Figure 11. Creep testing setup.

3. Results and Discussion

3.1. Compressive Strength

Figure 12 shows the compressive strength development of the AES-based AAM over time. The compressive strength of the samples increased logarithmically with curing time. It reached approximately 38 MPa (5500 psi) after 28 days of curing, comparable to the 28-day compressive strength of normal Portland cement pastes without additional heated curing. This binder also features relatively high early age strength, which is desirable for accelerated construction. The compressive strength of the AES-based AAM reached approximately 28 MPa (4000 psi) after three days, about 70% of the 28-day strength.

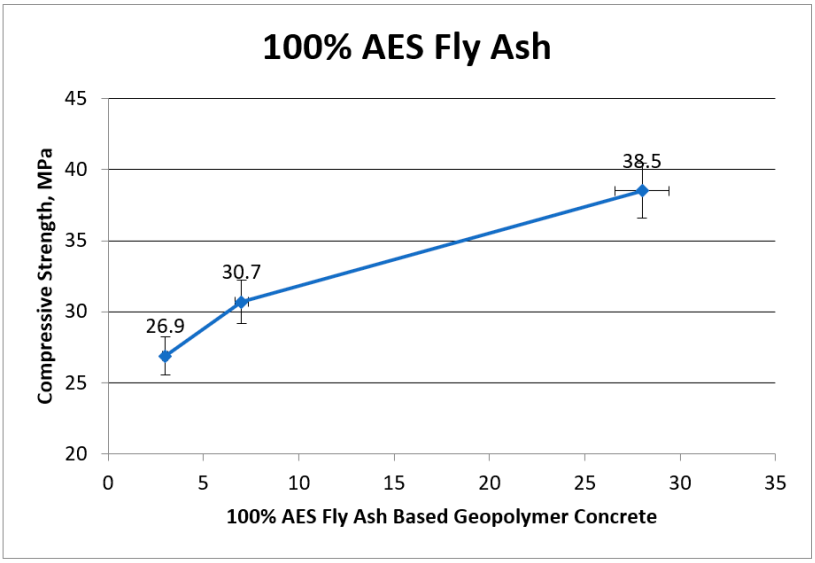

Figure 12. Compressive strength of the AES-based AAM cured for 3, 7, and 28 days.

In the case of using class F fly ash with lower amounts of calcium oxide, the compressive strength development of the geopolymer concrete in the early ages was reported to be relatively lower than OPC concrete; however, the later age strengths were significantly higher [17]. In contrast, the strength development of AES fly ash with a high content of calcium showed a relatively high 3-day compressive strength (26.9 MPa). The reason is probably due to the additional formation of C-S-H (calcium silicate hydrate) that coexisted with N-A-S-H (sodium aluminosilicate hydrate) in the alkali-activation process [18].

3.2. Drying Shrinkage

Drying shrinkage values of OPC, commercial fly ash (class F)-based AAM, and AES fly ash-based AAM mortars were conducted in accordance with ASTM C157, and the results are shown in Figure 13. Class F fly ash AAM mortar had the highest drying shrinkage of 0.090% at 14 days and 0.084% at 120 days. The drying shrinkage of OPC mortar was 0.030% at 14 days, and 0.07% at 120 days. The drying shrinkage of AES mortar samples was 0.0870% at 14 days and 0.075% at 120 days, similar to the class F fly ash AAM mortar. After two months, all three samples showed no changes in length.

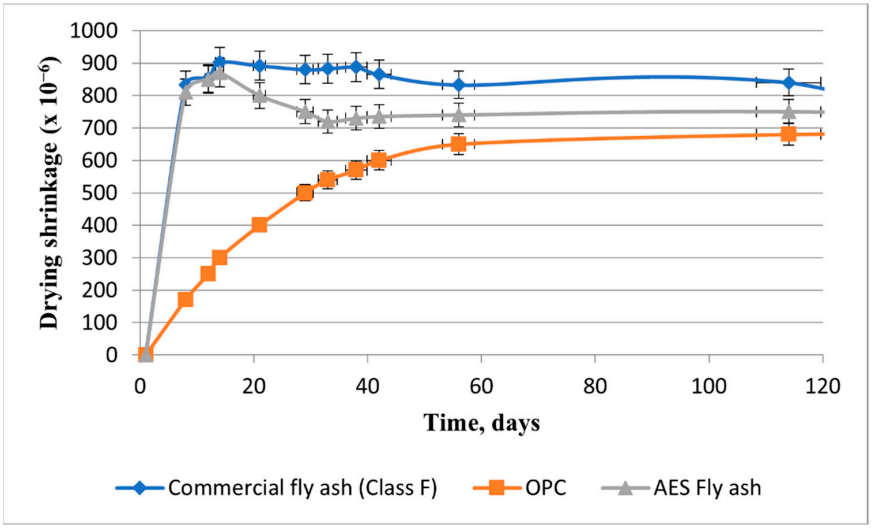

Figure 13. Drying shrinkage of OPC, commercial fly ash (class F)-based AAM, and AES fly ash- based AAM mortars.

Neupane et al. also reported that the drying shrinkage results of class F fly ash/GGBS-based AAMs were higher than the drying shrinkage of conventional concretes [17]. This behavior could be ascribed to the formation of a calcium aluminosilicate hydrate matrix [19]. AES fly ash has reactive calcium and alumina which could be released during the extended dissolution process employed in this study, leading to the formation of C-S-H and C-A-S-H.

3.3. Sulfate Attack

This durability test was conducted to determine the effects of the exposure to sulfates. Sulfates may come from groundwater or seawater and cause the expansion and cracking of concrete.

The compressive strength evolution of concrete specimens placed in sodium sulfate and magnesium sulfate solutions was studied. Strength reductions in specimens are shown in Figures 14 and 15 for sodium sulfate and magnesium sulfate exposure, respectively. In sodium sulfate-rich environments, the strength reduction in OPC was significantly higher compared to the AAM samples, which showed virtually no strength reduction.

After 12 months, the strength reduction for OPC concrete was 25% in the sodium sulfate solution and 37% in the magnesium sulfate solution, while AAM concrete had virtually no strength reduction in the sodium sulfate solution and 41% reduction in the magnesium sulfate solution. For both the OPC and AAM samples, strength reduction was higher in the magnesium sulfate than in the sodium sulfate solution.

Higher expansions in the OPC samples could be explained by the excess ettringite caused by the reaction between aluminates and sulfates [20]. Low strength loss of AES-based AAM samples may be explained by the absence of C_3A and portlandite, in addition to the formation of ettringite during hydration in the OPC samples. Wang et al. [21] also found that AAMs showed better durability performances than OPC-based materials in general.

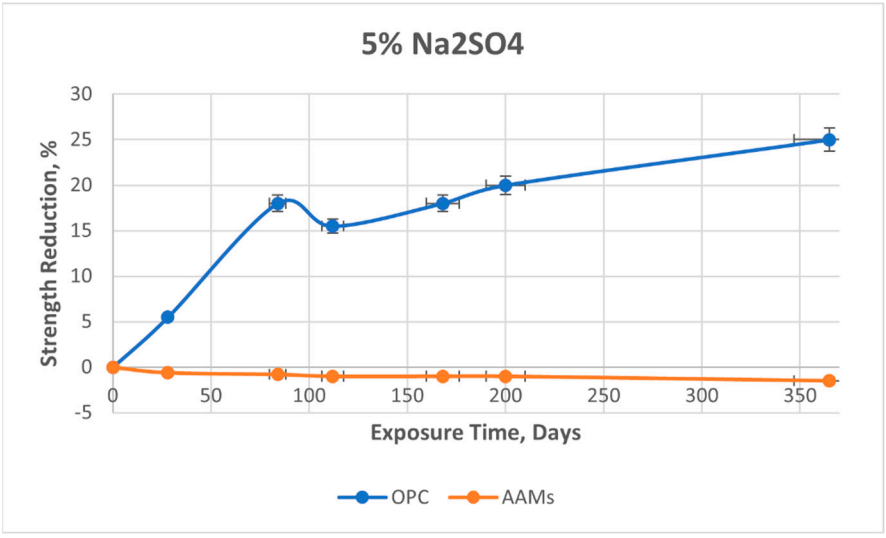

Figure 14. Strength reduction in OPC and AES fly ash AAM samples subjected to sodium sulfate attack for up to 365 days.

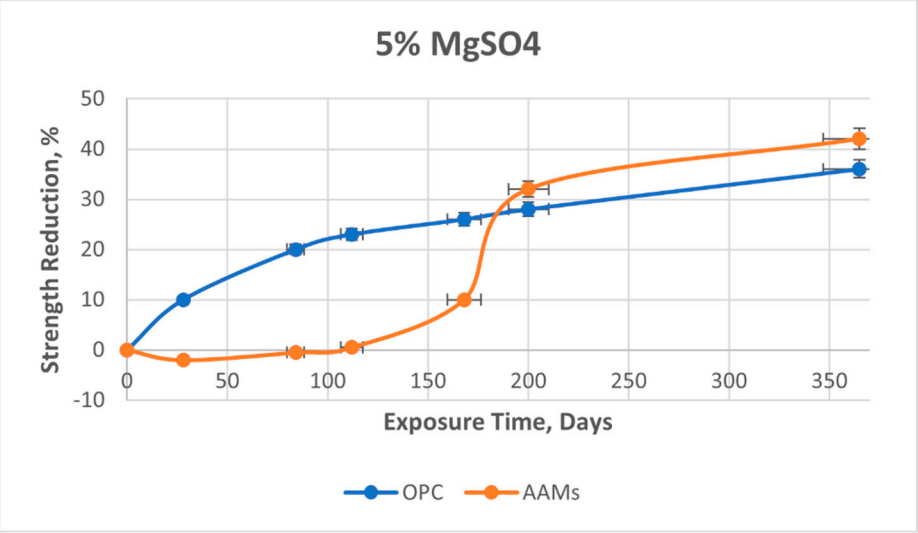

Figure 15. Strength reduction in OPC and AES fly ash AAM samples subjected to magnesium sulfate attack for up to 365 days.

In AAM samples, some loss in strength was observed when comparing samples stored in water with samples under $MgSO_4$ attack. In summary, under sodium sulfate attack, AAM concrete performed better than OPC concrete. In fact, the AAM samples even showed a little increase in strength with time in the sodium sulfate solution, and no significant strength loss in the magnesium sulfate solution until four months of exposure. However, the OPC samples showed significant losses in strength in both solutions.

XRD analysis of the AAM and OPC mortar samples showed different degradation products. In the AAM samples after one year of exposure, no gypsum or ettringite were present in the sample exposed to the Na_2SO_4 solution. In contrast, a considerable amount of gypsum was present in samples exposed to the $MgSO_4$ solution. Meanwhile, in the OPC samples, ettringite was present in the sample exposed to the Na_2SO_4 solution, and considerable amounts of ettringite and gypsum were found in the sample exposed to $MgSO_4$ [22]. It should be indicated that the study used type I/II Portland cement in the OPC samples. Different results may be expected if sulfate-resistant cement was used.

3.4. Alkali–Silica Reactions

Alkali content of the binder is critical for potential alkali–aggregate reactions (AAR) in Portland cement concrete [23]. As a subcategory of AAR, alkali–silica reactions (ASR) take place between potentially reactive aggregates and the alkalis present in cement, Na_2O, K_2O, and $Ca(OH)_2$. The reaction product is an alkali–silica gel that swells after absorbing moisture and can cause expansion and cracking in the concrete.

In the OPC concrete, the danger of ASR reactions could be reduced by limiting the alkali content of the concrete. A typical restriction is that the alkali content should not exceed 0.6 wt.% cement (where the K_2O content is included on a mortar equivalency basis) by weight of the cement. However, in AAMs, the alkali content is much higher than in OPCs due to the use of a significant amount of alkali for the activation of slag or fly ash in manufacturing the AAMs. For example, for alkali-activated slag cement (AAS), the amount of alkali reaches 2–5% [24].

Furthermore, due to the low calcium content of precursors, such as fly ash, alkali-activated binders based on these materials might be expected to exhibit a different behavior than OPCs. One possible reason is that the role of calcium in the ASR process is known to be important in determining the rate and extent of potentially deleterious processes [25].

Although alkali-activated slag (AAS) cement is lower in calcium than OPC and characterized by the absence of $Ca(OH)_2$ (which is considered beneficial), the concentration of alkalis in these binders is high; usually, over 3%, while OPC usually contains less than

0.8% $Na_2O_{eq.}$ This leads to concerns that such a high alkali content may promote ASR when reactive aggregates are used [26]. However, it should be noted that when alkalis are chemically combined in the reaction products rather than remaining entirely free in the pore solutions [27,28], or when high levels of reactive alumina are available (either directly from aluminosilicate precursors or through the addition of Al-rich components such as metakaolin) [29], this danger is reduced.

This investigation aimed to determine the effects of ASR on AAMs using an aggregate known to be reactive. An aggregate from Waikoloa, Hawaii, was found to be highly reactive and showed expansion above the ASTM C1260 limits for normal OPC concrete [30]. Figure 16 shows the AAM samples under ASTM C1260 in a 1 N NaOH solution.

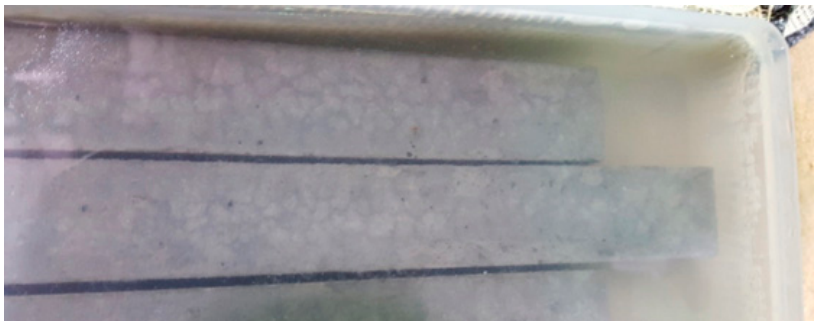

Figure 16. AAM samples for the ASR test (ASTM C1260) in a 1 N NaOH solution.

Results of the expansion tests, as per ASTM C1260, for mortar bar specimens immersed in 1 N NaOH solution are presented in Figure 17. The OPC specimens showed an average expansion of 0.25% after 14 days, exceeding the ASTM threshold (0.1%). The expansion value after a 28-day exposure to sodium hydroxide solution was 0.5%. At the end of the 28-day exposure, the AAM specimens only exhibited an expansion of 0.05%, which did not exceed the ASTM threshold of 0.1%. The expansion values for the OPC specimens were ten times greater than the AAM counterparts following 28 days of exposure. The high expansion values observed for the OPC specimens suggested that the aggregates used in this study were indeed deleterious.

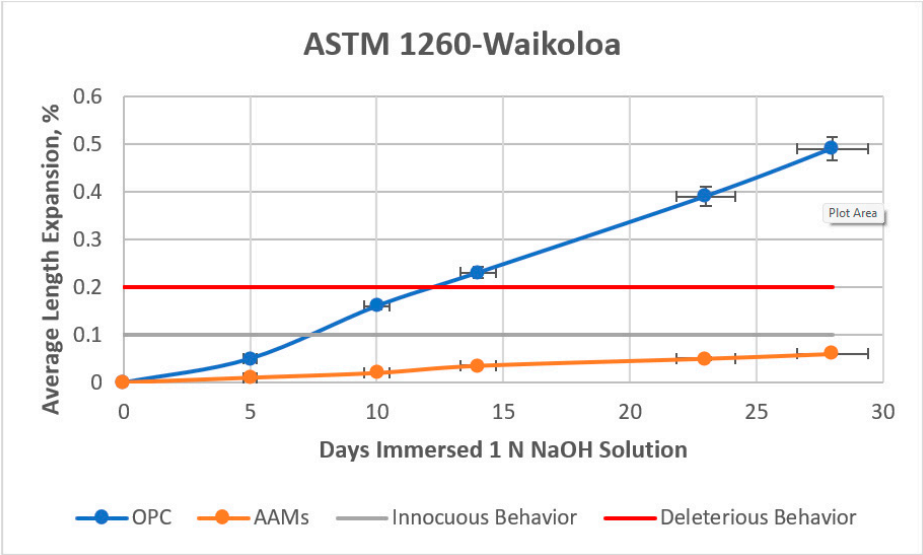

Figure 17. Expansion mortar specimens prepared using AAMs and OPC.

Other studies also reported that AAM samples developed less ASR expansion than OPC samples subjected to the accelerated mortar bar test as per ASTM C1260. Kupwade-

Patil and Allouche [31] using one type of class C and two types of class F fly ashes showed that OPC samples exhibited a higher average expansion, by a factor of six, compared to GPC specimens following a 90-day exposure to 1 N NaOH solution at 80 °C. OPC specimens made with sandstone, quartz, and limestone aggregates exceeded the permissible threshold (0.1%) for expansion specified by ASTM C1260. Puertas et al. [32] used three types of aggregates (siliceous, non-reactive calcareous, and reactive (dolomitic) calcareous), and compared the expansion of OPC and sodium silicate-activated slag (AAS) mortars. For a test duration of four months, OPC samples with siliceous aggregates revealed an expansion four times greater than that of the corresponding AAS when both were exposed to ASTM C1260 test conditions.

3.5. Creep Testing

Creep testing was conducted on the novel mix to determine the long-term deformation of alkali-activated mixes (AAMs) with high impurity contents. The test was conducted under loading to verify whether excessive deflection behavior was present. This test is also known as load-induced time-dependent compressive strain. Excessive deflection may lead to cracking, which could cause other undesirable durability issues. Figure 18 illustrates the setup for the creep test.

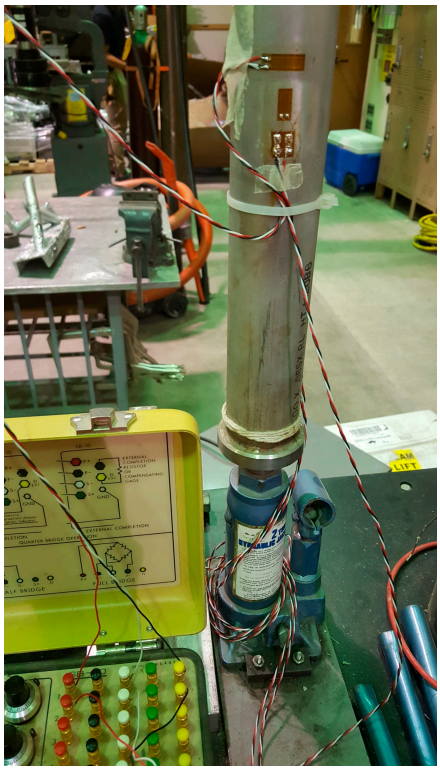

Figure 18. Setup for the creep test.

The creep behavior of AAM samples was compared with OPC samples under the standard creep test. Figure 19 shows the creep of the AAM and OPC samples for up to 180 days. Both series of creep data were loaded at the age of 28 days. The creep of the AAM specimens at 180 days of loading was roughly 600 micro-strains, which is smaller than the 700 micro-strains for the OPC specimens with the same grade of compressive strength.

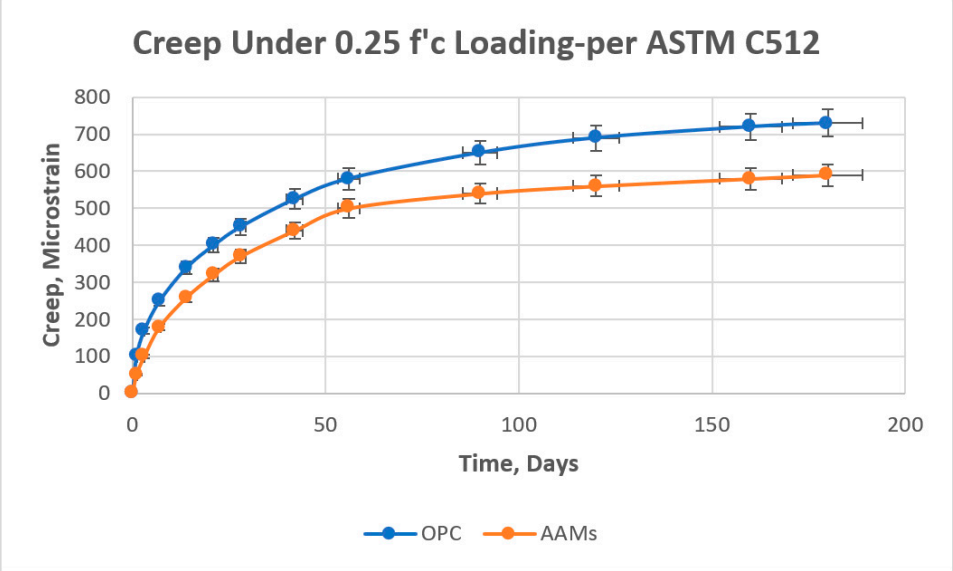

Figure 19. The creep strain data of the ambient-cured AAMs and OPCs.

It is interesting to note that the creep behaviors differed between the AAMs and OPCs. In general, the AAM specimens exhibited a lower creep than the OPC specimens, and the creep rate of the AAMs stabilized sooner at earlier ages (Figure 9). A finite ultimate creep for the OPC samples could not be confidently anticipated within the test period of 180 days, and the OPC samples yielded even higher creep than AAMs at later ages.

Collins and Sanjayan [33] reported in situ strength and strain results from measurements on an 800 × 800 × 1200 mm column composed of AAMs produced at a concrete plant. It was found that OPC concrete columns experienced more cracking and creep than AAM columns. Although calcium silicate hydrate (C-S-H) is the primary binding phase of cement-based and alkali-activated materials fabricated with high calcium contents, such as AES fly ash, the nature of C-S-H formed in the two materials may be different. Li and Zhang [34] implicated that concrete creep under service loads is contributed to by the intergranular preferential re-orientation of C-S-H nanocrystallites, not interlayer sliding or silicate chains explaining the differences in creep values.

4. Practical Implementation of the Novel Mixing Procedure

Samples prepared using the new mixing procedure had drastically improved rheology and were formable enough to flow and fill molds. A critical improvement the new mixing procedure provided is that the sodium hydroxide solution will have sufficient time to dissolve the impurities of the precursors and release the desired amounts of calcium, alumina, and silica ions. As important reactive components of the alkali-activation process, released calcium, alumina, and silica ions will be ready to form C-S-H and (N)-A-S-H, as the primary and secondary products. Introducing sodium silicate as the final step would provide soluble silica contributing to strength development. In contrast, taking traditional mixing steps leads to the early formation of gypsum with low strength that would interfere with the proper occurrence of C-S-H/N-A-S-H bonds.

Poon et al. [35] used calcium sulfate anhydrite ($CaSO_4$) to activate an AAM system. They found that a large quantity of ettringite (Aft) was formed during the early stage of hydration. This could be the main reason for the higher early age compressive strength of AES-based AAMs studied in this research. $CaSO_4$ was the common component in Poon's work and the current investigation. The key difference is that $CaSO_4$ was an external source in Poon's study, while $CaSO_4$ was part of the AES fly ash in the present research.

Manzi et al. [36] used different types of fly ash with different amounts of unburned carbon to fabricate mortar samples. Serious workability problems were reported when fly ash with a high carbon content was used. In order to avoid preliminary treatments

to eliminate the unburned matter, various methods were used such as changing the water/binder ratio, changing the ratio of the alkaline activators, and using different types of superplasticizers. Results showed that a high amount of unburned carbonaceous matter may not only compromise rheological and mechanical properties but also make it necessary to develop specific additives for the binder. Comparing the present research with the study mentioned above reveals the potential benefit of the novel mixing procedure to produce AAM concrete with excellent rheological and mechanical properties.

Although the utilization of fly ash with high impurities such as $CaSO_4$ and unburned carbon as a partial replacement for cement is not currently acceptable in the construction industry, this study shows that fabricating AAMs with precursors containing impurities could be an economical and environmentally friendly replacement for OPC concrete. The short-term and durability tests showed that this type of AAM is suitable to be used as a construction material. Therefore, the novel mixing procedure presented in this study may be recommended for AMM concretes using precursors with high impurity contents.

5. Conclusions and Future Research

Robust AAMs were developed in this study using a novel mixing procedure. Despite high contents of impurities, such as calcium sulfate and unburned carbon, the precursor is a potential replacement for OPC to produce high-performance AAMs at room temperature. The research studied the short- and long-term mechanical properties of AAM samples, and the results were compared with OPC concrete properties. The performance of AAM made from precursor with high impurity contents was satisfactory, and the main conclusions are as follows.

(1) A new mixing procedure has been developed by monitoring the dissolution process of precursors using Raman spectroscopy. The new method could significantly enhance the properties of HI-AAM, including fresh and hardened properties, as well as the durability. The dissolution time should be selected based on the type and amount of impurity. In the specific case of AES fly ash, the suitable dissolution duration was around 10 min;
(2) The hardened HI-AAM samples exhibited a reasonable 28-day compressive strength (38 MPa) and rapid strength gain (28 MPa at 3 days);
(3) HI-AAM demonstrated acceptable long-term properties:
    i. The drying shrinkage of HI-AAM samples conducted in accordance with ASTM C157 was comparable to that of normal concrete after four months (730×10^{-6});
    ii. Samples exposed to a sulfate-rich environment were tested in accordance with ASTM C1012. HI-AAM was virtually immune in a 5% sodium sulfate environment, in which conventional OPC deteriorated significantly after one year of exposure (25% decrease in compressive strength). Neither conventional concrete nor HI-AAM were immune to a 5% magnesium sulfate solution;
    iii. In the accelerated ASR test (ASTM 1260), HI-AAM specimens did not exceed the threshold of 0.1% (0.07%). Expansion values for the OPC specimens, however, were found to be seven times (0.49%) greater than those of their AAM counterparts following 28 days of exposure to NaOH;
    iv. Creep testing was conducted in accordance with ASTM C512 for 180 days of loading. The creep of HI-AAM specimens was about 600 micro-strains, which was smaller than the 700 micro-strains for the OPC specimens.

The satisfactory performances of the HI-AAMs imply the potential suitability of precursors with high impurity contents for a host of structural and non-structural concrete applications.

The short-term and durability tests showed that AAMs made from precursors with a high impurity content may be a suitable alternative to OPC. The novel mixing procedure presented in this study may be recommended for AAMs using precursors with high impurity contents. Due to the great potential benefits of the novel mixing procedure, future

studies are suggested to further optimize the mixing procedure by expanding the study to precursors with various types and amounts of impurities.

Author Contributions: Conceptualization, L.S.; methodology, L.S. and R.M.; validation, R.M., L.S. and I.J.; formal analysis, I.J., L.S. and R.M.; investigation, I.J.; data curation, R.M. and I.J.; writing—original draft preparation, R.M.; writing—review and editing, L.S., R.M. and B.W.; visualization, I.J. and R.M.; supervision, L.S.; project administration, L.S.; funding acquisition, L.S. All authors have read and agreed to the published version of the manuscript.

Funding: This research was funded by Hawaii Department of Transportation—TA 2013-3R.

Institutional Review Board Statement: Not applicable.

Informed Consent Statement: Not applicable.

Data Availability Statement: All data has been provided in the context of the manuscript.

Conflicts of Interest: The authors declare no conflict of interest.

References

1. Sundaresan, S.; Ramamurthy, V.; Meyappan, N. Improving Mechanical and Durability Properties of Hypo Sludge Concrete with Basalt Fibres and SBR Latex. *Adv. Concr. Constr.* **2021**, *12*, 327–337.
2. Divyah, N.; Prakash, R.; Sivakumar, A. Parametric Study on Lightweight Concrete-Encased Short Columns under Axial Compression-Comparison of Design Codes. *Struct. Eng. Mech.* **2022**, *83*, 387–400.
3. Prakash, R.; Thenmozhi, R.; Raman, S.N. Mechanical Characterisation and Flexural Performance of Eco-Friendly Concrete Produced with Fly Ash as Cement Replacement and Coconut Shell Coarse Aggregate. *Int. J. Environ. Sustain. Dev.* **2019**, *18*, 131–148. [CrossRef]
4. Mirmoghtadaei, R.; Shen, L. Design of Alkali-Activated Materials Based on Quantitative Microanalysis of Precursors and Reaction Kinetics. Ph.D. Thesis, University of Hawaii, Honolulu, HI, USA, 2020.
5. Li, Y.; Shen, L.; Mirmoghtadaei, R.; Ai, L. A Statistical Model on the Performance of Fly Ash-Based Geopolymer Concrete. In Proceedings of the Civil Engineering Conference in the Asian Region, Oahu, HI, USA, 30 August–2 September 2016.
6. Li, Y.; Shen, L.; Mirmoghtadaei, R.; Ai, L. A Design of Experiment Approach to Study the Effects of Raw Material on the Performance of Geopolymer Concrete. *Adv. Civ. Eng. Mater.* **2017**, *6*, 20160007. [CrossRef]
7. Duxson, P.; Provis, J.L. Designing Precursors for Geopolymer Cements. *J. Am. Ceram. Soc.* **2008**, *91*, 3864–3869. [CrossRef]
8. Dombrowski, K.; Buchwald, A.; Weil, M. The Influence of Calcium Content on the Structure and Thermal Performance of Fly Ash Based Geopolymers. *J. Mater. Sci.* **2007**, *42*, 3033–3043. [CrossRef]
9. Shi, J.; Liu, Y.; Xu, H.; Peng, Y.; Yuan, Q.; Gao, J. The Roles of Cenosphere in Ultra-Lightweight Foamed Geopolymer Concrete (UFGC). *Ceram Int.* **2022**, *48*, 12884–12896. [CrossRef]
10. Shi, J.; Tan, J.; Liu, B.; Chen, J.; Dai, J.; He, Z. Experimental Study on Full-Volume Slag Alkali-Activated Mortars: Air-Cooled Blast Furnace Slag versus Machine-Made Sand as Fine Aggregates. *J. Hazard. Mater.* **2021**, *403*, 123983. [CrossRef]
11. Wallah, S.E.; Rangan, B.V. Low-Calcium Fly Ash-Based Geopolymer Concrete: Long-Term Properties. Ph.D. Thesis, Curtin University of Technology, Perth, Australia, 2006.
12. Rashad, A.M. A Comprehensive Overview about the Influence of Different Admixtures and Additives on the Properties of Alkali-Activated Fly Ash. *Mater. Des.* **2014**, *53*, 1005–1025. [CrossRef]
13. Pangdaeng, S.; Phoo-ngernkham, T.; Sata, V.; Chindaprasirt, P. Influence of Curing Conditions on Properties of High Calcium Fly Ash Geopolymer Containing Portland Cement as Additive. *Mater. Des.* **2014**, *53*, 269–274. [CrossRef]
14. Alomayri, T.; Shaikh, F.U.A.; Low, I.M. Mechanical and Thermal Properties of Ambient Cured Cotton Fabric-Reinforced Fly Ash-Based Geopolymer Composites. *Ceram. Int.* **2014**, *40*, 14019–14028. [CrossRef]
15. Pacheco-Torgal, F.; Castro-Gomes, J.P.; Jalali, S. Investigations on Mix Design of Tungsten Mine Waste Geopolymeric Binder. *Constr. Build. Mater.* **2008**, *22*, 1939–1949. [CrossRef]
16. Temuujin, J.; van Riessen, A.; Williams, R. Influence of Calcium Compounds on the Mechanical Properties of Fly Ash Geopolymer Pastes. *J. Hazard. Mater.* **2009**, *167*, 82–88. [CrossRef]
17. Neupane, K.; Kidd, P.; Chalmers, D.; Baweja, D.; Shrestha, R. Investigation on Compressive Strength Development and Drying Shrinkage of Ambient Cured Powder-Activated Geopolymer Concretes. *Aust. J. Civ. Eng.* **2016**, *14*, 72–83. [CrossRef]
18. Phoo-ngernkham, T.; Phiangphimai, C.; Intarabut, D.; Hanjitsuwan, S.; Damrongwiriyanupap, N.; Li, L.Y.; Chindaprasirt, P. Low Cost and Sustainable Repair Material Made from Alkali-Activated High-Calcium Fly Ash with Calcium Carbide Residue. *Constr. Build. Mater.* **2020**, *247*, 118543. [CrossRef]
19. Kiran Ramagiri, K.; Kar, A.; Kara De Maeijer, P.; Rodriguez Sanchez, J. Experimental Determination, Correlation with Microanalyses, and Development of Simplified Prediction Models for Drying Shrinkage of Alkali-Activated Concrete. *J. Mater. Civ. Eng.* **2022**, *34*, 04022161. [CrossRef]

20. Diaz Caselles, L.; Hot, J.; Cassagnabère, F.; Cyr, M. External Sulfate Attack: Comparison of Several Alternative Binders. *Mater. Struct./Mater. Constr.* **2021**, *54*, 216. [CrossRef]
21. Wang, A.; Zheng, Y.; Zhang, Z.; Liu, K.; Li, Y.; Shi, L.; Sun, D. The Durability of Alkali-Activated Materials in Comparison with Ordinary Portland Cements and Concretes: A Review. *Engineering* **2020**, *6*, 695–706. [CrossRef]
22. Bakharev, T.; Sanjayan, J.G.; Cheng, Y.B. Sulfate Attack on Alkali-Activated Slag Concrete. *Cem. Concr. Res.* **2002**, *32*, 211–216. [CrossRef]
23. Helmuth, R.; Stark, D.; Diamond, S.; Moranville-regourd, M. Alkali-Silica Reactivity: An Overview of Research. *Concrete* **1993**, *108*, 202.
24. Chen, Y.Z.; Pu, X.C.; Yang, C.H.; Ding, Q.J. Alkali Aggregate Reaction in Alkali Slag Cement Mortars. *J. Wuhan Univ. Technol. Mater. Sci. Ed.* **2002**, *17*, 60–62+69.
25. Leemann, A.; Le Saout, G.; Winnefeld, F.; Rentsch, D.; Lothenbach, B. Alkali-Silica Reaction: The Influence of Calcium on Silica Dissolution and the Formation of Reaction Products. *J. Am. Ceram. Soc.* **2011**, *94*, 1243–1249. [CrossRef]
26. Provis, J.; van Deventer, J. (Eds.) *Alkali Activated Materials State-of-the-Art Report, RILEM TC 224-AAM*, 1st ed.; Springer: Cham, Switzerland, 2014; ISBN 978-94-024-0278-0.
27. Fernández-Jiménez, A.; Puertas, F. The Alkali-Silica Reaction in Alkali-Activated Granulated Slag Mortars with Reactive Aggregate. *Cem. Concr. Res.* **2002**, *32*, 1019–1024. [CrossRef]
28. Gruskovnjak, A.; Lothenbach, B.; Holzer, L.; Figi, R.; Winnefeld, F. Hydration of Alkali-Activated Slag: Comparison with Ordinary Portland Cement. *EMPA Act.* **2006**, *34*, 119–128. [CrossRef]
29. Krivenko, P.V.; Petropavlovsky, O.; Gelevera, A.; Kavalerova, E. Alkali-Aggregate Reaction in the Alkali-Activated Cement Concrete. In Proceedings of the 4th International Conference on Non-Traditional Cement & Concrete, Brno, Czech Republic, 27–30 June 2011.
30. Robertson, I.; Shen, L. Field Evaluation of Concrete Using Hawaiian Aggregates for Alkali Silica Reaction. In Proceedings of the MATEC Web of Conferences, Hualien, Taiwan, 31 October 2018; EDP Sciences: Ulysses, France, 2018; Volume 199.
31. Kupwade-Patil, K.; Allouche, E.N. Impact of Alkali Silica Reaction on Fly Ash-Based Geopolymer Concrete. *J. Mater. Civ. Eng.* **2013**, *25*, 131–139. [CrossRef]
32. Puertas, F.; Palacios, M.; Gil-Maroto, A.; Vázquez, T. Alkali-Aggregate Behaviour of Alkali-Activated Slag Mortars: Effect of Aggregate Type. *Cem. Concr. Compos.* **2009**, *31*, 277–284. [CrossRef]
33. Collins, F.; Sanjayan, J.G. Strength and Shrinkage Properties of Alkali-Activated Slag Concrete Placed into a Large Column; Cem. *Concr. Res.* **1999**, *29*, 659–666. [CrossRef]
34. Li, J.; Zhang, W. Preferred Orientation of Calcium Silicate Hydrate and Its Implication to Concrete Creep. *Compos. B Eng.* **2022**, *247*, 110297. [CrossRef]
35. Poon, C.S.; Kou, S.C.; Lam, L.; Lin, Z.S. Activation of Fly Ash/Cement Systems Using Calcium Sulfate Anhydrite (CaSO4). *Cem. Concr. Res.* **2001**, *31*, 873–881. [CrossRef]
36. Manzi, S.; Saccani, A.; Baldazzi, L.; Lancellotti, I. Mix-Design and Properties of Mortars from Alkali-Activated Fly Ashes Containing High Amounts of Unburned Carbon Matter. *Int. J. Concr. Struct. Mater.* **2020**, *14*, 59. [CrossRef]

Disclaimer/Publisher's Note: The statements, opinions and data contained in all publications are solely those of the individual author(s) and contributor(s) and not of MDPI and/or the editor(s). MDPI and/or the editor(s) disclaim responsibility for any injury to people or property resulting from any ideas, methods, instructions or products referred to in the content.